Cell. Mol. Life Sci. (2015) 72:1363–1375
DOI 10.1007/s00018-014-1747-4

Cellular and Molecular Life Sciences

RESEARCH ARTICLE

Functional and pharmacological induced structural changes of the cystic fibrosis transmembrane conductance regulator in the membrane solved using SAXS

Debora Baroni · Olga Zegarra-Moran · Oscar Moran

Received: 7 May 2014 / Revised: 18 September 2014 / Accepted: 26 September 2014 / Published online: 2 October 2014
© Springer Basel 2014

Abstract The cystic fibrosis transmembrane conductance regulator (CFTR) chloride channel is a membrane-integral protein that belongs to the ATP-binding cassette superfamily. Mutations in the CFTR gene cause cystic fibrosis in which salt, water, and protein transports are defective in various tissues. To investigate the conformation of the CFTR in the membrane, we applied the small-angle x-ray scattering (SAXS) technique on microsomal membranes extracted from NIH/3T3 cells permanentely transfected with wild-type (WT) CFTR and with CFTR carrying the ΔF508 mutation. The electronic density profile of the membranes was calculated from the SAXS data, assuming the lipid bilayer electronic density to be composed by a series of Gaussian shells. The data indicate that membranes in the microsome vesicles, that contain mostly endoplasmic reticulum membranes, are oriented in the outside-out conformation. Phosphorylation does not change significantly the electronic density profile, while dephosphorylation produces a significant modification in the inner side of the profile. Thus, we conclude that the CFTR and its associated protein complex in microsomes are mostly phosphorylated. The electronic density profile of the ΔF508-CFTR microsomes is completely different from WT, suggesting a different assemblage of the proteins in the membranes. Low-temperature treatment of cells rescues the ΔF508-CFTR protein, resulting in a conformation that resembles the WT. Differently, treatment with the corrector VX-809 modifies the electronic profile of ΔF508-CFTR membrane, but does not recover completely the WT conformation. To our knowledge, this is the first report of a direct physical measurement of the structure of membranes containing CFTR in its native environment and in different functional and pharmacological conditions.

Keywords CFTR · Phosphorylation · Membrane structure · ΔF508 rescue · Cystic fibrosis · Small angle X-ray scattering

Introduction

The cystic fibrosis transmembrane conductance regulator protein (CFTR) is an anion channel, whose mutations, including those that lead to misfolding and loss of channel activity, cause cystic fibrosis (CF). CFTR is a member of the ABC (ATP-binding cassette) transporter family. The architecture of CFTR consists of two transmembrane domains, each linked to a nucleotide-binding domain (NBD). These two motifs are connected by a regulatory domain (RD), which requires phosphorylation by PKA to allow the activation of the channel. The opening and closing of the channel (gating) are modulated by the association and hydrolysis of ATP by the NBDs. This means that activation and gating of the channel involve conformational modifications in the intracellular part of the protein that provide the power stroke for opening and closing the channel.

Little is known about the structure of the whole CFTR protein, and how phosphorylation and ATP modulate the

Electronic supplementary material The online version of this article (doi:10.1007/s00018-014-1747-4) contains supplementary material, which is available to authorized users.

D. Baroni · O. Moran (✉)
Istituto di Biofisica, CNR, via De Marini, 6, 16149 Genoa, Italy
e-mail: oscar.moran@cnr.it

O. Zegarra-Moran
Unità Operativa di Genetica Medica, Istituto G. Gaslini, Genoa, Italy

opening of the channel. Furthermore, there is only partial understanding of how the mutation ΔF508 (the most common in humans) affects the structure and folding of the protein. Like many other mammalian membrane proteins, full-length CFTR has proven to be difficult to purify because of its low expression levels and the requirement of detergents to render the protein soluble in aqueous solutions. Electron microscopy (EM) two-dimensional crystals and single-particle analysis have permitted to discriminate, at low resolution, two different conformational states, probably representing the open and closed states of the channel [1, 2]. Also, some structural changes associated with phosphorylation, nucleotide binding, and channel gating have been obtained by EM of the whole CFTR [3, 4], and small-angle x-ray scattering (SAXS) of isolated recombinant RD [5]. Also ATP-binding associated conformational changes of the NBDs have been observed by SAXS experiments of isolated recombinant NBDs [6, 7]. However, the only structural data available at atomic resolution of CFTR come from recombinant NBDs [8–10].

To address the conformational characterisation of CFTR in its native environment, a lipidic membrane, we have investigated the structural features of microsomal membranes extracted from cells over-expressing the wild-type (WT) or the pathological mutant ΔF508. The study was performed using the SAXS method, that is a well-established technique that has traditionally been used for the ensemble solution of the structure of biomolecules [11, 12], of large and regular-shaped structures, such as virus capsids [13], ribosomes [14], and synaptic vesicles [15]. Using this technique, we estimated the electronic density profile of membranes expressing WT or mutant CFTR under different experimental conditions.

The aims of these experiments were, first, to determine the effects of phosphorylation on the electronic density profile of membranes containing CFTR. Second, we aimed to assess the structural characteristics of the microsomal membranes extracted from cells expressing the folding conformers of the ΔF508 mutant and investigate whether the rescue of the ΔF508-CFTR protein, pharmacologically or by low-temperature treatment, modifies the electronic density profile of the membranes. We present here the first direct physical evidence that WT and ΔF508 CFTR differently contribute to the structure of the membrane.

Materials and methods

Cell cultures

NIH/3T3 cells, either untransfected (null), permanently transfected with the WT human CFTR or with the CF mutant ΔF508 were grown as a monolayer culture at 37 °C in a CO2 incubator that provided a humidified environment (95 % air and 5 % CO2). The three cell lines were grown in Dulbecco's Modified Eagle's Medium supplemented with 2 mM L-glutamine and 10 % FBS. Cultures were grown in 875 cm^2 polystyrene flasks (Corning, Tewksbury, MA, USA). The medium was changed on day 3 after plating, and every 2 days thereafter. All culture media components were purchased from Sigma-Aldrich (St. Louis, MO, USA).

Two further ΔF508-transfected cell preparations were performed with rescue treatments. Prior to membrane extraction, cells were kept for 48 h at 27 °C or were incubated with 3 μM of VX-809 (Lumacaftor, Selleck Chemicals, Huston, TX, USA) for 48 h.

Membrane extraction

Microsomal membranes were prepared by a standard differential centrifugation protocol [16, 17]. Cells from 3 to 4 multilayer flasks (875 cm^2 surface), grown to >80 % confluence, were washed twice with ice-cold phosphate buffer saline (PBS, in mM: 2.7 KCl, 1.5 KH_2PO_4, 136.9 NaCl, 8.9 Na_2HPO_4, pH 7.4), trypsinized and pelleted at 600 g. Cells were resuspended in 6 ml of ice-cold hypotonic lysis buffer (HEPES 10 mM, EDTA 1 mM, pH 7.2) supplemented with protease inhibitors (phenylmethylsulfonyl fluoride 0.5 mM, N-p-Tosyl-L-alanine chloromethyl ketone 0.1 mM and N-p-Tosyl-L-lysine chloromethyl ketone 0.1 mM), and incubated for 10 min in ice. The suspension was lysed with 10 strokes in a chilled Dounce homogeniser; 6 ml of Sucrose Buffer (HEPES 10 mM, sucrose 500 mM, pH 7.2) was added to the lysate, and further 15 strokes were applied. The homogenate was centrifuged at 6500 g for 5 min to separate nuclei and cell debris from the supernatant that was recovered and centrifuged at 100,000 g for 45 min. The microsomal pellet was resuspended in 100–500 μl of storage buffer (HEPES 10 mM, sucrose 250 mM, $MgCl_2$ 5 mM, pH 7.2), fast-frozen in liquid N_2, and kept at −80 °C until used.

SDS-PAGE and Western blot

Protein concentration was determined using the method of Bradford [18], using bovine serum albumin as the standard. Equal amounts of proteins (15 μg) were subjected to 5 % SDS polyacrylamide gel electrophoresis. The gel was stained with Comassie Blue R-250 for 4 h and destained in 40 % methanol, 10 % acetic acid, and 50 % H_2O until background became clear. Separated proteins were also transferred to PVDF membrane (Millipore, Billerica, MA, USA) for 1 h. Blots were incubated with anti-CFTR

monoclonal antibody (1:1,000; clone MM13-4, Millipore) as primary antibody, and with horseradish peroxidase-conjugated goat anti-mouse antibody (1:4,000; Santa Cruz), as secondary antibody. In order to confirm the homogeneity of the loaded proteins, immunoblots were stripped by incubating them with stripping buffer (62.5 mM TRIS–HCl pH = 6.8, 10 % SDS and 1 % β-mercaptoethanol) for 30 min at 55 °C and re-probed with an anti-calnexin mouse monoclonal antibody (1:2,000, Abcam, Cambridge, UK), which is an endoplasmic reticulum marker [19].

Microsomal membrane samples (15 μg) were also separated on 6 % SDS–polyacrylamide gels and transferred onto PVDF membranes. Membranes were blocked using milk protein and probed with anti-calnexin (1:500, Abcam), anti-pan cadherin (1:1,000, Abcam) or anti-GM130 (1:200, BD Bioscience, San José, CA, USA) primary antibodies, which are endoplasmic reticulum, plasma membrane [20, 21] and cis-Golgi markers [22], respectively. Quantification of the samples was carried out using Quantity One software (Bio-Rad). The relative expression of membrane samples was normalised to the expression of NIH/3T3 whole cell lisate samples. In all experiments, immunodetection was performed using Amersham ECL PLUS detection reagents and the images were captured by using Amersham Hyperfilm ECL. Each experiment was conducted in triplicate.

Sample preparation

Samples were thawed immediately before use and protein concentration was estimated using the method of Bradford using bovine serum albumin as the standard. The catalytic fraction of protein kinase A (PKA, Sigma-Aldrich) at a concentration of 600 units per nM of protein, supplemented with 50 μM of ATP, was added to an aliquot of the preparations to phosphorylate the membrane proteins. The mixture was incubated for 30–40 min at 37 °C. Dephosphorylation was obtained by incubation of samples with 5 units of alkaline phosphatase per μg of protein for 30–40 min at 37 °C. Enzymes were added to the membrane samples during thawing, when vesicles were not yet formed, to ensure their contact with both sides of the membranes.

All samples, untreated native, phosphorylated and dephosphorylated membranes, were dialysed by using 0.1 ml Mini Dialysis Devices (3.5 K MWCO, Thermo Scientific Pierce Protein Biology Products, Rockford, IL USA) against 500 ml of PBS and without ATP. The dialysis solution was further used as a blank buffer for SAXS experiments. Samples used for SAXS had a protein concentration between 2.14 and 5.13 mg/ml (average 3.70 mg/ml).

SAXS data collection

Small-angle X-ray scattering spectra of membranes were collected at the BL-11 beam line of the ALBA Synchrotron Light Facility (Barcelona, Spain). Scattered radiation was recorded in a two-dimensional CCD detector. The sample-detector distance of 2.39 m covered the range of momentum transfer $0.14 < q < 4.5$ nm^{-1} ($q = 4\pi \sin(\theta)/\lambda$, where 2θ is the scattering angle and $\lambda = 0.1$ nm is the X-ray wavelength; the optical path of the X-ray through the sample is about 3 mm). Data were collected from samples kept at 10 °C. For each sample, we recorded 40 spectra of 5 s each, corresponding to a total of 3.3 min of data acquisition. Dithiotreitol (5 mM) was added as free radical scavenger to minimise the radiation damage of the samples. The CCD camera images arisen from the random orientation of vesicles were integrated radially, resulting in the so-called '*I*–*q* plot', a one-dimensional profile of X-ray intensity $I(q)$ versus scattering vector q. The comparison of ten successive exposures of an acquisition experiment indicated no changes in the scattering patterns, i.e., no measurable radiation damage to the protein samples. The scattering data of the dialysis buffer, tested before and after each corresponding sample measured, were averaged and used to subtract the background.

Data analysis

The structure of the membranes was inferred from their electronic density profiles calculated from the SAXS spectra. In these experiments, the measured X-ray intensity is an average over a polydisperse vesicle population according to Debye scattering theory [23] such that

$$\langle I(q)\rangle = N\langle F(q)^2\rangle + \sum^{N} \cos(q\mathbf{r}_{\mathbf{nn}'}) \quad (1)$$

where $F(q)$ is the bilayer form factor, N is the number of particles (vesicles) and $\boldsymbol{r}_{\mathbf{nn}'}$ is the inter-vesicle vector. The first term of Eq. (1) represents the average scattering of N individual vesicles, while the second term comes from the interference between vesicles and depends on the distance between them, $\boldsymbol{r}_{\mathbf{nn}'}$. Because of the low vesicle concentration used in this study, no interference between vesicles is expected [24]. In fact, scattering coming up from the second term becomes significant at $q \ll 0.001$ nm^{-1} [24] that is beyond of the q range utilised here. Thus, the second term of Eq. (1) could be neglected, and we can use the simple relation

$$\langle I(q)\rangle \propto \langle F(q)^2\rangle, \quad (2)$$

where N is included in the arbitrary instrumental scaling. The form factor, $F(q)$, is the Fourier transform of the electronic density $\rho(r)$ of the bilayer.

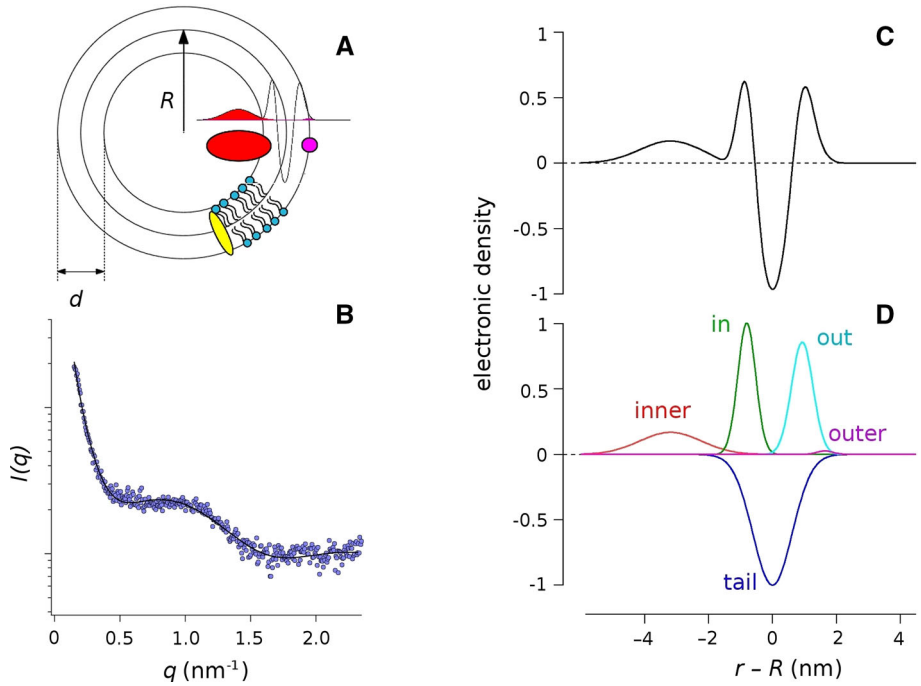

Fig. 1 Analysis of the SAXS data of membranes extracted from cells transfected with WT-CFTR. **a** Sketch of the model of a vesicle of radius *R*, consistent with the measured SAXS data. The wall of the vesicle of thickness *d* is formed by a lipid bilayer and integral membrane proteins (pictured in yellow). The electronic density profile is completed by the contribution of the inner and outer decorations (depicted in red and magenta, respectively). **b** SAXS spectra of the WT-CFTR microsomal membranes, showing the plot of the integrated scattered intensity $I(q)$ versus scattering vector q. The electronic density profile (**c**) was calculated from the five Gaussian model, according to Eq. (3). The decomposition of each singular Gaussian used to model the electronic density is shown in **d**. The parameters used to calculate the electronic density resulted from the best fit of the SAXS spectra with Eq. (5) (*continuous line* in **b**)

To calculate the electronic density we constructed a model of the membrane and adjusted the parameters of the model to fit its Fourier transform to the experimental SAXS spectra. EM showed that microsomal membranes form closed unilamellar vesicles (Supplementary Figure 5), as observed also in other microsomal fraction preparations [25, 26]. The electronic density of the vesicle wall can be described by five concentric Gaussian shells [15, 24, 27, 28] that include an asymmetric bilayer profile with added decorations on the inner and outer sides of the vesicle wall (Fig. 1). The bilayer electronic density profile is modelled by two positive Gaussians, representing the headgroups of the two lipid leaflets (*in* and *out*, respectively) and a negative Gaussian representing the hydrophobic core (*tail*; see Fig. 1). Note that amino acid residues associated with lipid headgroups and transmembrane protein segments are included in these contributions. The parts of the proteins extending beyond the bilayer towards the internal or external sides of the vesicle (*inner* and *outer* protein shells in Fig. 1) are modelled by concentric Gaussians attached to the inner and outer sides of the bilayer, respectively. The electronic density of the bilayer profile as a function of the distance r is given by

$$\rho(r) = \sum_{k=1} \rho_k \exp\left[\frac{-(r-\delta_k)^2}{2\sigma_k^2}\right] \tag{3}$$

with the peak position δ_k, amplitude ρ_k, and width σ_k with $k \in$ *in, out, tail, inner, outer*, for each of the three Gaussians representing the headgroups of the two leaflets and the phospholipid tail region, and the inner and outer protein shell, respectively. The radius R is the distance defined from the centre of the vesicle to δ_{tail}. Thus, we define $\varepsilon_k = \delta_k - R$, and, therefore, $\varepsilon_{\text{tail}} = 0$. The membrane thickness is characterised by the total thickness d of the bilayer structure:

$$d = [\varepsilon_{\text{in}} - \sigma_{\text{in}}\sqrt{2\pi}] - [\varepsilon_{\text{out}} + \sigma_{\text{out}}\sqrt{2\pi}] \tag{4}$$

SAXS data allow to measure the scattering contrast $\Delta\rho = \rho(r) - \rho_{\text{solvent}}$. This analysis provides the relative amplitudes of each bilayer feature, not the absolute amplitudes, and the magnitude of ρ_{solvent} is arbitrary and set equal to zero. The electronic density of the two peaks representing the headgroups was defined to be $\rho_{\text{in,out}} > 0$, and the peak that represents the lower electronic density of the bilayer, plausibly corresponding to the methyl groups of the phospholipids was fixed to $\rho_{\text{tail}} = -1$ [29]. These

two assumptions reduced the parameter dependency of the fitting procedure and also provided a means of comparing the models since all results were normalised to the central region of the bilayer. Notice that the Gaussians representing the bilayer profile and the protein shells inter-penetrate to some extent.

For a perfectly spherical, radially symmetric vesicle composed of n Gaussian shells, the form factor $\langle F(q)^2\rangle = F(q)F(q)^*$ is obtained from the radially symmetric Fourier transform of Eq. (3). We used a normalised ensemble average over $F(q)^2$ [24, 28], resulting in

$$\langle F(q)^2\rangle = \zeta\left\{\frac{1}{q^2}\sum_{k,k'}(R+\varepsilon'_k)\rho_k\rho'_k\sigma_k\sigma'_k \times \exp[-q^2(\frac{\sigma_k^2+\sigma_{k'}^2}{2})]\cos[q(\varepsilon_k-\varepsilon'_k]\right\}, \quad (5)$$

where $F(q)^2$ is the form factor and ζ is a proportionality factor. Note that Eq. (5) is an approximation valid only in the region $0.1 > q > 10\ \mathrm{nm}^{-1}$, where intensity arising from intra-bilayer features dominates the scattering curve. The derivation of the expression in Eq. (5), obtained from a normalized ensemble average over $F(q)2$ utilising a Gaussian weight to describe the distribution of vesicles with radii R', average radius R, and standard deviation σR, is described in the Appendix A of the article of Brzustowicz and Brunger [24]. The data fitting procedure utilised the non-linear, least-squares Levenberg–Marquardt fitting (NLSF) algorithm to minimise χ^2 (IgorPro, Wavemetrics, Lake Oswego, OR, USA):

$$\chi^2 = \sum_j \frac{I(q)-\hat{I}(q)^2}{\sigma(q_j)} \quad (6)$$

where $\hat{I}(q_j)$ is a fitted value (model value) for q_j, $I(q_j)$ is the measured data value for the jth point, and $\sigma(q_j)$ is an estimate of the standard deviation for $I(q_j)$. The goodness of the fit was characterised by the correlation coefficient r^2. The electronic density profile of the lipid vesicle wall was obtained with high accuracy fitting the model over the experimental data. This method allows also having a good estimate of the average vesicle radius.

Results

CFTR in membranes

Experiments were carried on the cellular microsomal fractions that contain mainly endoplasmic reticulum vesicles, Golgi fragments, plasma membrane and, in minor amount, other intracellular membranes [30, 31]. We performed a Western blot analysis of the microsomal membranes to asses their content (Fig. 2). The immunoreactivity of the microsomal membranes for each subcellular marker was compared with that of the total cell lysate (first lane of each blot in Fig. 2). In our samples, we found a content of calnexin, the endoplasmic reticulum marker, between 78 and 81 % with respect to its content in NIH/3T3 whole cell lisate (Fig. 2a). The relative content of the plasma membrane marker, cadherin, and the cis-Golgi apparatus marker, GM130, was between 36 and 38 % and between 26 and 31 %, respectively (Figs. 2b, c). These values represent the fraction of each membrane class that was recovered in the microsomal membranes. Notice that the relative amount of each membrane class in the microsomal fraction was quite constant in each preparation.

To estimate the actual composition of our microsomal preparations, we used the estimation of the membrane fractions of different cells. The analysis of the distribution of organelle membranes in whole cells, determined by morphometric methods, in hepatocytes [32, 33], CH cells [34], and in RTL cells [35], yielded an average content of endoplasmic reticulum of 34 %, Golgi apparatus of 6 %, and plasma membrane of 7 %. Given that the amount of other membrane components is negligible in microsomal membranes [30, 31], it could be argued that microsomes are composed by 86 % of endoplasmic reticulum, 7 % of Golgi, and 7 % of plasma membrane.

The Western-blot experiment presented in Fig. 3a shows that microsomal membranes extracted from NIH/3T3 cells permanently transfected with WT-CFTR (lane 2) exhibit the dominant presence of the mature form of the protein (band C) and a minor amount of the immature form of CFTR (band B). Differently, microsomal membranes extracted from untransfected cells do not show any immunoreactivity to CFTR-antibodies (see Fig. 2a, lane 1). The lower panel in Fig. 3a shows the immunoreactivity of the same samples to the anti-calnexin antibody, confirming the homogeneity of the loaded membrane samples. The Coomassie 250R stained gel displayed in Fig. 3b clearly shows the presence of CFTR in the microsomal membranes extracted from NIH/3T3 cells permanently transfected either with WT- or ΔF508-CFTR (lanes 3 and 4, respectively). On the contrary, no band corresponding to CFTR molecular weight was detected in microsomal membranes extracted from control NIH/3T3 untransfetced cells (lane2). Consistently, there are evident differences between the SAXS data obtained from microsomal membranes without CFTR and the spectra from microsomal membranes containing CFTR (see Supplementary Figure 1).

The electronic density profiles in Fig. 4 were calculated adjusting the parameters of the model described in Eq. (3) to fit the SAXS spectra with the Fourier transform of the model shown in Eq. (5). Fitting parameters are presented in Supplementary Table 1. The best fits of SAXS data were

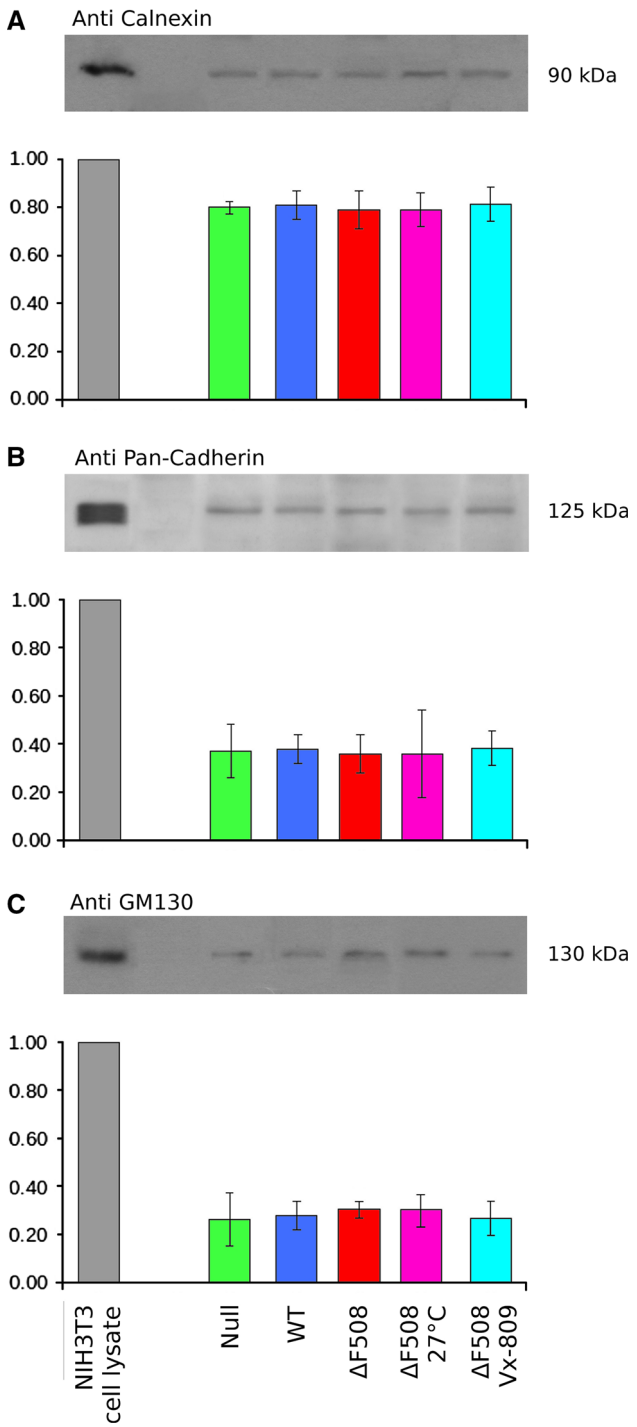

Fig. 2 Detection of endoplasmic reticulum-marker, calnexin (**a**), the plasma membrane-marker, cadherin (**b**), and the Golgi apparatus-marker, GM130 (**c**). The bands represent NIH/3T3 whole cell lisate (lane 1), and microsomes from untransfected NIH/3T3 cells (lane 3), cells expressing the WT-CFTR (lane 4), cells expressing the CFTR mutant ΔF508 (lane 5), cells expressing the CFTR mutant ΔF508 and incubated at 27 °C (lane 6), and cells expressing the CFTR mutant ΔF508 and treated with VX-809 (lane 7). The graphics below each Western blot image represent the detection of the different markers in each microsomal membrane sample, normalised to the expression of NIH/3T3 whole cell lisate. Each experiment was done in triplicate

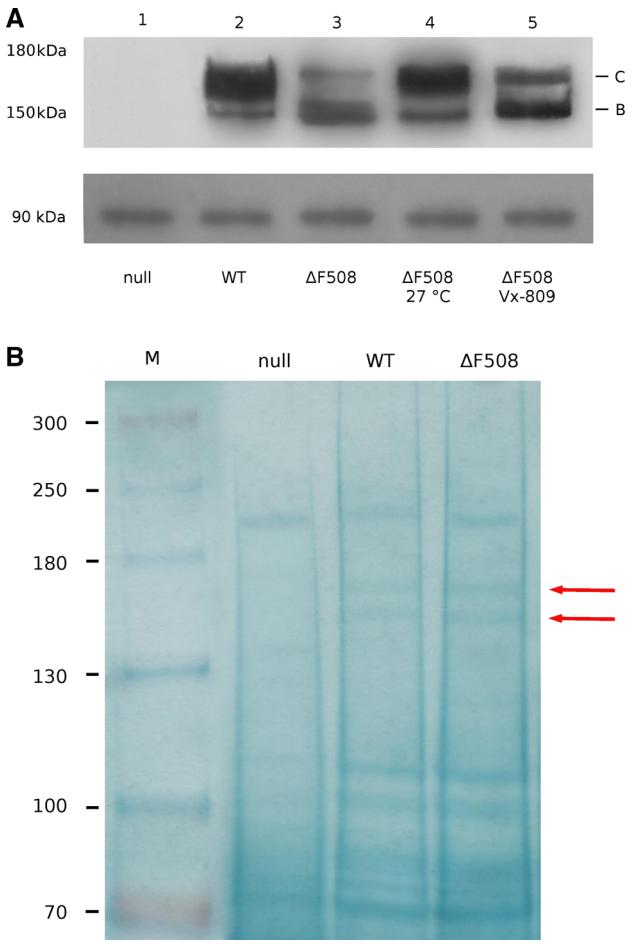

Fig. 3 **a** Western-blot analysis of membranes of untransfected NIH/3T3 cells (lane 1), cells expressing the WT-CFTR (lane 2), untreated cells expressing the CFTR mutant ΔF508 (lane 3), cells expressing the CFTR mutant ΔF508 and incubated at 27 °C (lane 4), and cells expressing the CFTR mutant ΔF508 and incubated with VX-809. The upper panel shows the immunoreactivity of the membranes to the anti-CFTR antibody, and the lower panel the immunoreactivity of the same membranes to the anti-calnexin antibody. **b** Comassie R250 stained gel of membranes extracted from untransfected NIH/3T3 cells (lane 2), cells expressing the WT-CFTR (lane 3), and untreated cells expressing the CFTR mutant ΔF508 (lane 4). The molecular protein ladder is showed in the first lane together with the molecular mass (in kDa) of its protein bands. The arrows indicate the bands corresponding to the molecular weights in which the mature glycosylated and the immature core-glycosylated forms of transfected CFTR proteins should be localised

obtained for an average vesicle radius of 72.5 nm and 82.2 nm, for null and WT-CFTR microsomal membranes, respectively. The vesicle radii have similar dimensions to those observed by EM (Supplementary Figure 5) and in other microsomal preparations [25, 26].

At first glance, the electronic density profiles in Fig. 4 appear asymmetric with quite different decorations at the surfaces of the bilayers. The amount of material at the inner surface of the membrane ($r < 0$) is significantly larger.

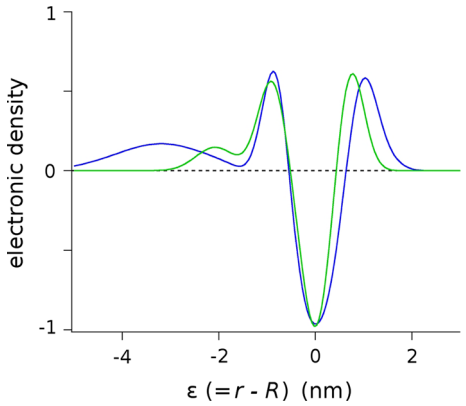

Fig. 4 Electronic density profiles of membranes extracted from untransfected NIH/3T3 cells (*green*) and NIH/3T3 cells transfected with WT-CFTR (*blue*). It is worth noting that shifts of the density peaks means a different distribution of material in that region of the membrane

This could be interpreted as a preferential orientation of the membrane-forming vesicles.

The thickness of the WT-CFTR microsomal membranes, as defined in Eq. (4), 3.28 nm, is bigger than that of the null membranes (3.03 nm). This difference is mainly caused by an increase of the electronic density in the external leaflet of the membrane (ρ_{out}) and by a more prominent decoration at the inner side of the WT-CFTR microsomal membranes, while decorations in the external leaflet of null membranes are near absent. This is consistent with a larger mass content of the membranes of transfected cells, likely due to the over-expression of CFTR. Interestingly, the higher mass excess is observed at the inner side of the membrane. Considering the topology of CFTR, where about 80 % of the protein is in the cytoplasmic side [36] and where CFTR interacts with a plethora of intracellular proteins [37–40], we could infer that most of the microsomal membranes in the vesicles probably adopt the outside-out orientation.

CFTR phosphorylation

To understand the role of phosphorylation on the conformation of CFTR and its associated protein complex, microsomal membranes were treated with PKA to obtain a full phosphorylation of the system, or with alkaline phosphatase, to study a completely dephosphorylated membrane. The enzymes used to phosphorylate or dephosphorylate the membranes (protein kinase A or alkaline phosphatase, respectively) were added at the beginning of the thawing of the samples, before the formation of the vesicles, to ensure their access to both sides of the membranes. Data obtained from WT-CFTR microsomal membranes were compared to null microsomal

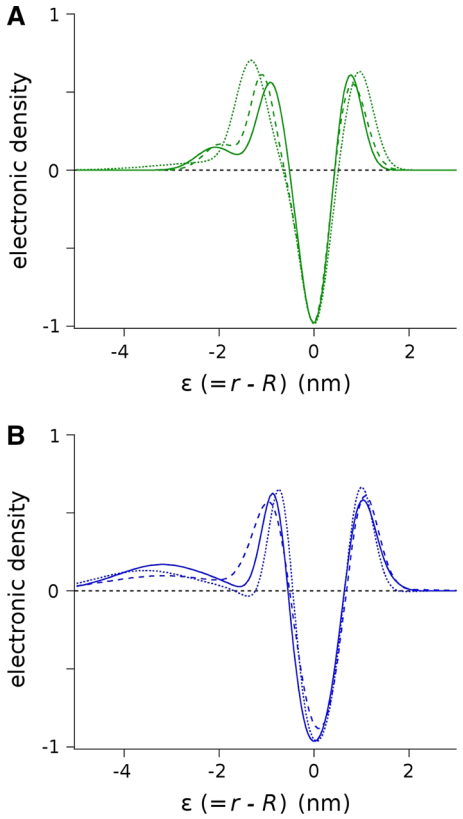

Fig. 5 The electronic density profiles of membranes extracted from untransfected NIH/3T3 cells (**a**), and cells transfected with WT-CFTR (**b**). Profiles were constructed from SAXS spectra of native (*continuous lines*), PKA-phosphorylated (*dotted lines*) and phosphatase-dephosphorylated membranes (*dashed lines*)

membranes. Both treatments introduced differences in the SAXS spectra of either null or WT-CFTR microsomal membranes, more pronounced in the inner side of the membrane (see Supplementary Figures 2 and 3).

Full phosphorylation causes a major modification of the electronic density profile of null-microsomal membranes (Fig. 5a dotted line). There is an increase of the electronic density peak in the internal leaflet of the membrane (ρ_{in}, see Supplementary Table 1), with a lost of the decorations on the surface of the membrane (reduced ρ_{inner}), and a 0.24 nm thickening of the lipid bilayer (from 3.03 nm of native membranes to 3.27 nm of full phosphorylated null microsomal membranes). Conversely, dephosphorylation (Fig. 5a, dashed line) ensues to a smaller modification of the electronic profile of null membranes, resulting on an electronic density profile similar to that of the native membranes (Fig. 5a, continuous line), with a minor re-accommodation of the inner decorations.

Differently, in WT-CFTR microsomal membranes full phosphorylation and dephosphorylation produce changes of the electronic density profile that are opposed to those observed in null membranes (Fig. 5b). PKA-

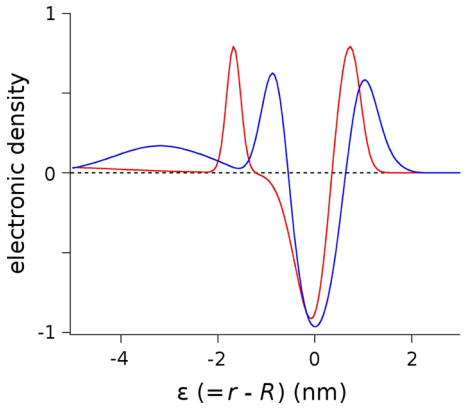

Fig. 6 Electronic density profiles of membranes extracted from NIH/3T3 cells transfected with ΔF508-CFTR (*red*). The electronic density profiles of the WT-CFTR membranes (*blue*) are shown for comparison

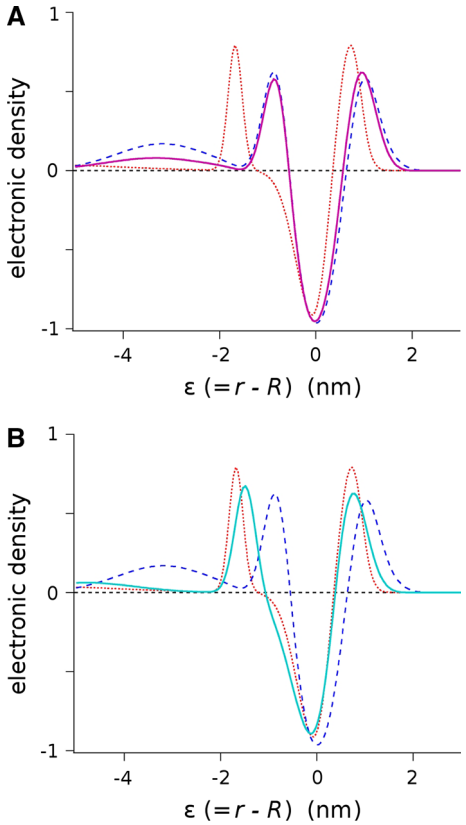

Fig. 7 Electronic density profiles of membranes from NIH/3T3 cells transfected with ΔF508-CFTR and incubated at 27 °C (**a**, *magenta*) and in the presence of 3 μM VX-809 (**b**, *cyan*). In both panels, the electronic density profiles of native WT-CFTR membranes (*blue dashed lines*) and of native ΔF508-CFTR membranes (*red dotted lines*) are shown for comparison

phosphorylation treatment modifies the aspect of the inner surface decoration, displacing it to the left, and narrowing the *in* and *out* high-density peaks on both sides of the membrane (Fig. 5b, dotted line). Vice versa, dephosphorylation of WT-CFTR microsomal membranes (dashed line) results in a widening of the inner decoration, with a displacement towards the membrane. These changes are accompanied by a broadening of the high electronic density peak at the internal leaflet of the membrane (Fig. 5b).

Membranes containing ΔF508-CFTR

Microsomal membranes extracted from cells expressing the CFTR mutant ΔF508 produced SAXS spectra that are significantly different from the spectra of WT-CFTR membranes (Supplementary Figure 1). The Western blot experiment (Fig. 3a, lane 3), showing a prominence of the immature form of the protein (band B), corroborated the presence of ΔF508-CFTR in the microsomal membranes. Indeed, the electronic density profile of the ΔF508-CFTR membranes is different from those obtained from the null membranes (compare Figs. 4, 6).

The electronic density model that fits the ΔF508-CFTR spectra is also significantly different from that of WT-CFTR microsomal membranes (Fig. 5). The bilayer thickness (3.27 nm) of ΔF508-CFTR was not significantly different from the WT-CFTR (3.28 nm), but the shape of the membrane was different. First, in the microsomes of the mutant CFTR cells, both leaflets of the membrane are displaced towards the inner side of the vesicle, and the two positive peaks, *in* and *out*, are narrower. Moreover, decorations at the inner side of the membrane are smaller, and those at the outer side of the vesicle are nonexistent. In addition, there is a shoulder in the aliphatic region of the internal leaflet, suggesting that high electronic density material has accommodated in the core of the membrane. These data suggest that the ΔF508 mutation introduces a major modification in the assemblage of proteins in the membrane, inducing the CFTR-associated proteins complex to accommodate into the membrane with a different topology than that interacting with WT-CFTR.

Rescue of the ΔF508-CFTR

Mutant ΔF508-CFTR produces a defect of the assemblage and maturation of CFTR, and a successive degradation of the protein, resulting in a lack of docking of functional CFTR at the plasma membrane. The correct trafficking of the mutant CFTR can be recovered by low-temperature treatment, as shown by the Western blot analysis of membranes extracted from NIH/3T3 cells incubated at 27 °C (Fig. 3a, lane 4). After the low-temperature treatment, there is a significant fraction of mature CFTR (band C), while a small fraction of ΔF508 remains immature (band B). Consistently, the SAXS spectra of ΔF508-CFTR microsomal membranes are significantly modified when

ΔF508-CFTR transfected cells are incubated at 27 °C (Supplemenary Figure 4).

Fit of experimental data to the multi-Gaussian shell model of low-temperature treated ΔF508-CFTR membranes resulted in an electronic density profile (continuous magenta line in Fig. 7a) that is completely different from that of native ΔF508-CFTR microsomal membranes (dotted red line), and noteworthy similar to the electronic density profile of WT-CFTR membranes (dashed blue line). The only remarkable difference with respect to the WT-CFTR microsomal membrane profile is that, in the low temperature rescued ΔF508-CFTR membranes, decorations at the inner surface of the membrane have a less pronounced electronic density (Fig. 7a).

Differently, the pharmacological treatment of ΔF508-CFTR transfected cells with the corrector VX-809 did not yield a similar rescue of the ΔF508 mutant. Figure 3a (lane 5) shows that the relative intensity of the mature CFTR band of the corrector-treated cells increased in comparison with that of the no-treated ΔF508-expressing cells, but most of the protein is still in its immature form (Fig. 3a). As a result of this incomplete rescue, the SAXS spectra of ΔF508-CFTR microsomal membranes treated with VX-809 are different from those of the untreated membranes (Supplementary Figure 4), but the electronic profile resulting from the multi-Gaussian shell model fit does not overlap the electronic density profile of the WT-CFTR membranes (Fig. 7b). When compared to untreated ΔF508-CFTR, membranes treated with VX-809 (continuous cyan line in Fig. 7b) show a widening of the *in* and *out* high-density peaks, and a slight increase of the electronic density at the inner side decorations. Also the shoulder in the internal leaflet, that characterises the ΔF508-CFTR microsomal membranes, almost disappears in VX-809 treated membranes (Fig. 7b). It is evident that improvement of maturation upon corrector treatment modifies the conformation of the complex formed by the mutant CFTR and its associated proteins, but the effect is not enough to get a membrane profile that resembles the WT-CFTR conformation.

Discussion

We have investigated the structure of membrane-derived microsomal vesicles prepared from NIH/3T3 cells transfected with WT- and ΔF508-CFTR. Microsomal membranes are organised forming unilamellar vesicles of relatively homogeneous dimensions [25, 26, 31], as confirmed by electron microscopy (Supplementary Figure 5). The cellular microsomal fraction contains mainly endoplasmic reticulum vesicles, Golgi fragments, plasma membrane and, in minor amount, other intracellular membranes [30, 31, 33]. A Western blot analysis confirmed this composition of the retrieved microsomal samples, showing the relative amount of each fraction with respect to NIH3T3 whole-cell lysate (Fig. 2). The composition of the microsomes was estimated considering an average measurement of the amount of each organelle by morphometric methods [32–35], yielding 86 % of endoplasmic reticulum, and 7 % of both, Golgi and plasma membrane.

Proteomic experiments have revealed differences in the interactors of CFTR and other proteins in various cell lines [37], likely reflecting tissue specific differences in folding, trafficking, function and regulation. These differences might show not only steady-state variations in cell trafficking patterns specific to cell or tissue types, but also the localization of CFTR in a particular sub-compartment at the time of complexes recovery [37, 40]. In our experimental conditions, because of the majority of the endoplasmic reticulum fraction (>85 %), the CFTR-associated protein complex largely reflects the interactions occurring in the endoplasmic reticulum.

Thus, microsomal vesicle membranes may contain WT-CFTR in the form in which it transits to the plasma membrane. This concept is confirmed by the high fraction of mature CFTR observed in the Western-blot experiments (Fig. 3a, lane 2). Differently, the ΔF508-CFTR, whose localization is normally limited to the endoplasmic reticulum membranes [54], was mostly detected as immature protein (Fig. 3a, lane 3). We focused the analysis on the structural features of these microsomal membrane fractions, describing the electronic density profiles of the membranes at a spatial resolution of 2.85 nm, calculated from the SAXS spectra. To corroborate the contribution of the CFTR on the electronic density profiles, we examined the differences between microsomal membranes obtained from cells expressing CFTR and microsomal membranes from untransfected cells (null) that do not show any immunoreactivity to the CFTR antibodies in the Western blot analysis (Fig. 3a, lane 1).

We performed SAXS experiments with suspensions of microsomal membranes. The random orientation of the membranes impeded a direct reconstruction of the electronic density, because the phases of the form factors could not be resolved. Therefore, we attempted to solve the structure from the opposite side, proposing an electronic density model that could fit the experimental data. To achieve this purpose and construct the electronic density profile, we used a multi-Gaussian shell model [15, 24, 28]. This type of model has been successfully used to estimate the structure of the vesicle wall of liposomes composed by different lipids [24, 28, 42, 43] and of synaptic vesicles [15, 27]. It has to be noticed that, even if the spatial resolution is relatively low, this is a method that allows the direct observation of the molecular conformation of the proteins

associated with membranes. Moreover, because of the nature of the sample preparation, it is possible to introduce perturbations to the system like direct application of drugs or modulators (like nucleotides) to observe the effect exerted on the configuration of the CFTR associated protein complex in its native environment (a cell membrane) without denaturating the proteins. This is a clear advantage of this method over other approaches.

When microsomal membranes were exposed to synchrotron X-rays, the resultant two-dimensional image acquired showed concentric rings, which arise from the average scattering of an ensemble of randomly oriented vesicles. The scattered intensities were measured from the radial integration of the images. Background, obtained from the scattering of the buffer used, was subtracted, yielding the I–q plots. After subtracting the background, the scattering arising solely from microsomal vesicles is shown in the Supplementary Figures 1–4.

The membrane wall structure was determined from the scattering theory, assuming the lipid bilayer electronic density, $\rho(r)$, to be composed by a series of five Gaussian shells [15, 24, 28]. Qualitatively, the calculated $\rho(r)$ produces the familiar shape of a vesicle lipid bilayer wall [15, 24, 28, 29, 43]. Experimental data were subjected to NLSF utilizing Fourier transform of the proposed model. We initially tried a "flat" model, where the fitting expression did not account for the spherical shape of the vesicle (data not shown), and a "symmetric" model, where the membrane leaflets were considered identical (data not shown). However, these models inadequately describe the observed data as indicated by the poor χ^2 and correlation coefficient values. Hence, we interpreted all our data using an asymmetric membrane wall model of spherical vesicles. Interestingly, the vesicle radius, computed as a free parameter in our calculations, resulted of the same order of magnitude of that measured in microsomal vesicles by EM (see Supplementary Figure 5) [25, 26].

It has been shown that CFTR interacts with a conspicuous number of proteins (http://string-db.org/) [37–40]. Thus, it is expected that the contribution of WT-CFTR in the electronic density profile of the membranes is determined by the over-expressed CFTR itself and by the interacting proteins. In fact, the comparison of the electronic density profile of the microsomal membranes containing WT-CFTR with the null microsomal membranes (Fig. 4) shows a larger contribution to the decorations at the bilayer surface, almost certainly due to the recruitment of an excess of proteins in CFTR membranes.

The electronic density profile of the microsomal vesicle membranes is characterised by a marked asymmetry. The contribution of the curvature to the asymmetry of vesicles with a radius of 70–83 nm would result on a difference of less than 3 % of the electronic density between the bilayer leaflets. Thus, the asymmetry of the lipid bilayer would be caused by an unequal distribution of molecules in the membrane. This characteristic is detectable only if most vesicles in suspension have the same membrane orientation. Therefore, we can conclude that membranes have a preferential orientation in the microsomal vesicles, where the inner leaflet of membranes has a higher electronic density, probably reflecting a higher protein content in the inner side of the vesicle. This statement is supported by the asymmetry of different microsomal vesicles observed by electron microscopy [25, 31, 44]. This fact is not surprising, considering that surface tensions may be different on each side of the membrane, conditioning the curvature, and the successive resealing of vesicles.

Nearly 80 % of the CFTR mass is located in the intracellular side, including the NBDs, the regulatory domain, the intracellular loops of the membrane spanning domains, and the N- and C-terminal domains [36]. Moreover, there is a large number of proteins that interact with the intracellular side of CFTR [37, 39, 40]. Thus, we can suppose that the membranes of the microsomal vesicles are oriented outside-out, that is, the cytoplasmic side of the CFTR and its associated protein complex are located in the inner part of the vesicle. In the experimental conditions used, i.e. in the absence of ATP, most probably CFTR channels are in the closed conformation.

A cardinal step of CFTR functioning is CFTR activation upon PKA-phosphorylation of the regulatory domain [36, 45–47]. Phosphorylation causes a conformational change in the regulatory domain [5, 48–50], modifying the interactions between this domain and the nucleotide-binding domains [49, 51]. Therefore, changing the phosphorylation conditions of CFTR is expected to induce a conformational modification in the intracellular side of the protein and, likely, a modification of the protein–protein interactions of the CFTR-associated protein complex. In addition, proteins associated with CFTR that could be susceptible to phosphorylation may be also affected, modifying the conformation of the complex.

Phosphorylation of WT-CFTR microsomal membranes induces a relatively small change in the electronic density profile (Fig. 5b, dotted line), mostly in the inner surface of the membrane, while dephosphorylation causes a more severe modification on the inner side of the membrane, with a reduction of the internal decoration and an enlargement of the inner peak (Fig. 5b, dashed line). These effects give rise to two conclusions. First, the fact that the larger effects of phosphorylation and dephosphorylation occur in the inner side of the membrane supports the notion that this side represents the intracellular side of the CFTR complex in the microsomal membrane. Second, the higher effect of dephosphorylation advocates in favour of the idea

that the native WT-CFTR is already partially phosphorylated. In null-microsomal membranes, phosphorylation has a higher effect on the electronic density profiles, and the effect is extended also to the outer side of the membrane, while the smaller effect of dephosphorylation on the inner high electronic density peak is similar to what occurs in WT-CFTR microsomal membranes (Fig. 5).

The most common CFTR mutation, ΔF508, causes the degradation of the protein before maturation and docking to the plasma membrane. Microsomal preparation captures the ΔF508-CFTR, mostly in the immature state (Fig. 3a, lane 3). It is, therefore, a good preparation to study the conformation of the mutant CFTR before undergoing degradation. Several studies have proposed that, in the endoplasmic reticulum, the conformation of ΔF508-CFTR is different from that of WT-CFTR, either in terms of stability or in domain–domain interactions [52–55]. We have confirmed such conformational differences by the direct comparison of the structure of ΔF508-CFTR membranes with WT-CFTR membranes. The electronic density profile of the microsomal membranes containing the mutant protein, that is significantly different from that containing WT-CFTR (Fig. 6), indicates that the number of interacting proteins is reduced in the ΔF508-CFTR [37], probably due to a different folding conformation of the mutant CFTR, as evident from the lack of the inner surface decorations that characterise the WT-membranes (Fig. 6). The different conformation of ΔF508-CFTR- associated protein complex in the microsomal membranes has probably an important role in vivo in the recognition, by the cell quality control system, of CFTR as an acceptable protein or a protein to be degraded.

The observation of a different conformation of the ΔF508 in the microsomal membrane rises also questions concerning the possibility of correcting the defect. Beside the important issue of compensating the trafficking towards the plasma membrane, the rescued ΔF508-CFTR should ideally also recover the appropriate functional conformation to exert its transport function. We have attempted two different methods to correct the ΔF508-CFTR defect. Low-temperature treatment has been extensively used as the prototype for correcting the ΔF508 processing and functional defects in vitro [56–58]. Incubation of ΔF508 transfected-cells at 27 °C rescued a significant amount of the ΔF508 protein as shown by band C of the Western blot analysis (Fig. 3a, lane 4) and by electronic density profiles that are very similar to those of the WT-CFTR microsomal membranes (Fig. 7a), indicating that this procedure causes also a significant recovery of the native structural conformation. Conversely, pharmacological treatment of cells with the corrector VX-809 resulted in microsomal membranes with an electronic density that was different not only from that of ΔF508-CFTR, but also from WT-CFTR membranes (Fig. 7b). While the shoulder in the inner leaflet that characterises the ΔF508-CFTR microsomal membranes almost completely disappeared and the two high-density peaks widened in microsomal membranes form VX-809 treated cells, the distance between the two high-density peaks resulted greater than in the WT-CFTR profile, and the inner side decoration characteristic of WT-CFTR microsomal membranes hardly increased. Two alternative hypotheses may explain this result. The first is that pharmacologically rescued ΔF508-CFTR can overcome the protein quality control machinery of the cell, reaching the plasma membrane, but its conformation is not completely rescued. A possible membrane destabilisation caused by the VX-809 itself [28] could contribute to this incomplete assemblage of the protein. This explanation would imply that VX-809 treated ΔF508-CFTR is still functionally defective [59–61]. Alternatively, VX-809 could have rescued the structural conformation of only a fraction of ΔF508 protein, as shown by band C in Fig. 2a, so that the electronic density profile is a weighted sum of corrected and non corrected protein. Nevertheless, the location of the small internal decoration, that remains far away from the lipid bilayer ($\varepsilon_{\text{inner}}$ is at -4.79 nm after VX-809 treatment, while it is −3.57 nm on phosphorylated WT-CFTR), indicates that the conformation reached by the ΔF508-CFTR-associated protein complex, when treated with VX-809, is still different from that of WT-CFTR.

Summarising, we present here the electronic density profiles of microsomal membranes containing CFTR to describe the structural configuration of the complex formed by this membrane protein and its associated interacting proteins in their native medium, a cell membrane. We have obtained evidence that WT-CFTR in microsomal membranes is partially phosphorylated, and the mutant ΔF508-CFTR-associated protein complex has a conformation that is very different from that of the WT-CFTR. We hypothesise that the differences between the WT and mutant CFTR-associated protein complexes may be caused primarily by a different conformation of the CFTR itself. Moreover, the treatment of mutant CFTR at 27 °C modifies ΔF508-membrane conformation, resulting in a structure more similar to WT-CFTR microsomal membranes. Differently, the pharmacological rescue of ΔF508-CFTR does not yield a complete recovery of the defective protein, either because the conformation obtained after VX-809 treatment is different from that obtained by incubation at low temperature, or because the amount of protein corrected is significantly lower. We cannot exclude, however, that some characteristics observed herein could be due to the over-expression of an heterologous protein. To our knowledge, this is the first report where a biophysical approach has been used to evaluate the structural conformational changes of WT and mutant CFTR protein

complex after physiological and pharmacological manipulation.

Acknowledgements This work was partially supported by the Fondazione per la Ricerca sulla Fibrosi Cistica, grant FFC#4/2012. These experiments were performed at the BL11-NCD beamline of ALBA Synchrotron Light Facility with financial support of the facility and the collaboration of ALBA staff. We thank Marc Malfois, Agneta Svenson and Christina Kamma-Lorger for the technical assistance at the synchrotron beamline. We are indebted to Dr. Cristina D'Arrigo for helping with the EM experiments. We thank also Alessandro Barbin for the construction of the sample cell for SAXS.

References

1. Awayn NH, Rosenberg MF, Kamis AB, Aleksandrov LA, Riordan JR, Ford RC (2005) Crystallographic and single-particle analyses of native- and nucleotide-bound forms of the cystic fibrosis transmembrane conductance regulator (CFTR) protein. Biochem Soc Trans 33:996–999
2. Rosenberg MF, Kamis AB, Aleksandrov LA, Ford RC, Riordan JR (2004) Purification and crystallization of the cystic fibrosis transmembrane conductance regulator (CFTR). J Biol Chem 279:39051–39057
3. Rosenberg MF, O'Ryan LP, Hughes G, Zhao Z, Aleksandrov LA, Riordan JR, Ford RC (2011) The cystic fibrosis transmembrane conductance regulator (CFTR): three-dimensional structure and localization of a channel gate. J Biol Chem 286:42647–42654
4. Zhang L, Aleksandrov LA, Zhao Z, Birtley JR, Riordan JR, Ford RC (2009) Architecture of the cystic fibrosis transmembrane conductance regulator protein and structural changes associated with phosphorylation and nucleotide binding. J Struct Biol 167:242–251
5. Marasini C, Galeno L, Moran O (2013) A SAXS-based ensemble model of the native and phosphorylated regulatory domain of the CFTR. Cell Mol Life Sci 70:923–933
6. Galeno L, Galfrè E, Moran O (2011) Small-angle X-ray scattering study of the ATP modulation of the structural features of the nucleotide binding domains of the CFTR in solution. Eur Biophys J 40:811–824
7. Galfrè E, Galeno L, Moran O (2012) A potentiator induces conformational changes on the recombinant CFTR nucleotide binding domains in solution. Cell Mol Life Sci 69:3701–3713
8. Atwell S, Brouillette CG, Conners K, Emtage S, Gheyi T, Guggino WB, Hendle J, Hunt JF, Lewis HA, Lu F, Protasevich II, Rodgers LA, Romero R, Wasserman SR, Weber PC, Wetmore D, Zhang FF, Zhao X (2010) Structures of a minimal human CFTR first nucleotide-binding domain as a monomer, head-to-tail homodimer, and pathogenic mutant. Protein Eng Des Sel 23:375–384
9. Lewis HA, Buchanan SG, Burley SK, Conners K, Dickey M, Dorwart M, Fowler R, Gao X, Guggino WB, Hendrickson WA, Hunt JF, Kearins MC, Lorimer D, Maloney PC, Post KW, Rajashankar KR, Rutter ME, Sauder JM, Shriver S, Thibodeau PH, Thomas PJ, Zhang M, Zhao X, Emtage S (2004) Structure of nucleotide-binding domain 1 of the cystic fibrosis transmembrane conductance regulator. EMBO J 23:282–293
10. Lewis HA, Zhao X, Wang C, Sauder JM, Rooney I, Noland BW, Lorimer D, Kearins MC, Conners K, Condon B, Maloney PC, Guggino WB, Hunt JF, Emtage S (2005) Impact of the DeltaF508 mutation in first nucleotide-binding domain of human cystic fibrosis transmembrane conductance regulator on domain folding and structure. J Biol Chem 280:1346–1353
11. Mertens HDT, Svergun DI (2010) Structural characterization of proteins and complexes using small-angle X-ray solution scattering. J Struct Biol 172:128–141
12. Stuhrmann HB (2008) Small-angle scattering and its interplay with crystallography, contrast variation in SAXS and SANS. Acta Crystallogr A 64:181–191
13. Sano Y, Inoue H, Kajiwara K, Hiragi Y, Isoda S (1997) Structural analysis of A-protein of cucumber green mottle mosaic virus and tobacco mosaic virus by synchrotron small-angle X-ray scattering. J Protein Chem 16:151–159
14. Svergun DI, Burkhardt N, Pedersen JS, Koch MH, Volkov VV, Kozin MB, Meerwink W, Stuhrmann HB, Diedrich G, Nierhaus KH (1997) Solution scattering structural analysis of the 70 S Escherichia coli ribosome by contrast variation. II. A model of the ribosome and its RNA at 3.5 nm resolution. J Mol Biol 271:602–618
15. Castorph S, Riedel D, Arleth L, Sztucki M, Jahn R, Holt M, Salditt T (2010) Structure parameters of synaptic vesicles quantified by small-angle x-ray scattering. Biophys J 98:1200–1208
16. Aleksandrov L, Mengos A, Chang X, Aleksandrov A, Riordan JR (2001) Differential interactions of nucleotides at the two nucleotide binding domains of the cystic fibrosis transmembrane conductance regulator. J Biol Chem 276:12918–12923
17. Gunderson KL, Kopito RR (1994) Effects of pyrophosphate and nucleotide analogs suggest a role for ATP hydrolysis in cystic fibrosis transmembrane regulator channel gating. J Biol Chem 269:19349–19353
18. Bradford MM (1976) A rapid and sensitive method for the quantitation of microgram quantities of protein utilizing the principle of protein-dye binding. Anal Biochem 72:248–254
19. Körschen HG, Yildiz Y, Raju DN, Schonauer S, Bönigk W, Jansen V, Kremmer E, Kaupp UB, Wachten D (2013) The non-lysosomal β-glucosidase GBA2 is a non-integral membrane-associated protein at the endoplasmic reticulum (ER) and Golgi. J Biol Chem 288:3381–3393
20. Kong E, Peng S, Chandra G, Sarkar C, Zhang Z, Bagh MB, Mukherjee AB (2013) Dynamic palmitoylation links cytosol-membrane shuttling of acyl-protein thioesterase-1 and acyl-protein thioesterase-2 with that of proto-oncogene H-ras product and growth-associated protein-43. J Biol Chem 288:9112–9125
21. Mondini A, Sassone F, Civello DA, Garavaglia ML, Bazzini C, Rodighiero S, Vezzoli V, Conti F, Torielli L, Capasso G, Paulmichl M, Meyer G (2012) Hypertension-linked mutation of α-adducin increases CFTR surface expression and activity in HEK and cultured rat distal convoluted tubule cells. PLoS One 7:e52014
22. Nakamura N, Rabouille C, Watson R, Nilsson T, Hui N, Slusarewicz P, Kreis TE, Warren G (1995) Characterization of a cis-Golgi matrix protein, GM130. J Cell Biol 131:1715–1726
23. Guinier A (1994) X-ray Diffraction in Crystals, Imperfect Crystals, and Amorphous Bodies. Courier Dover Publications, San Francisco and London
24. Brzustowicz MR, Brunger AT (2005) X-ray scattering from unilamellar lipid vesicles. J Appl Cryst 38:126–131
25. Wibo M, Amar-Costesec A, Berthet J, Beaufay H (1971) Electron microscope examination of subcellular fractions. 3. Quantitative analysis of the microsomal fraction isolated from rat liver. J Cell Biol 51:52–71
26. Lavoie C, Lanoix J, Kan FW, Paiement J (1996) Cell-free assembly of rough and smooth endoplasmic reticulum. J Cell Sci 109(Pt 6):1415–1425
27. Castorph S, Arleth L, Sztucki M, Vainio U, Ghosh SK, Holt M, Jahn R, Salditt T (2010) Synaptic vesicles studied by SAXS:

derivation and validation of a model form factor. J Phys Conf Ser 247:012015
28. Baroni D, Zegarra-Moran O, Svensson A, Moran O (2014) Direct interaction of a CFTR potentiator and a CFTR corrector with phospholipid bilayers. Eur Biophys J 43:341–346
29. Pabst G, Rappolt M, Amenitsch H, Laggner P (2000) Structural information from multilamellar liposomes at full hydration: full q-range fitting with high-quality X-ray data. Phys Rev E 62:4000–4009
30. De Duve C (1971) Tissue fractionation past and present. J Cell Biol 50:20d–55d
31. Palade GE, Siekevits P (1956) Liver microsomes: an integrated morphological and biochemical study. J Biophys Biochem Cytol. 2:171–200
32. Blouin A, Bolender RP, Weibel ER (1977) Distribution of organelles and membranes between hepatocytes and nonhepatocytes in the rat liver parenchyma. A stereological study. J Cell Biol 72:441–455
33. Croze EM, Morré DJ (1984) Isolation of plasma membrane, golgi apparatus, and endoplasmic reticulum fractions from single homogenates of mouse liver. J Cell Physiol 119:46–57
34. Saeger W, Rübenach-Gerz K, Caselitz J, Lüdecke DK (1987) Electron microscopical morphometry of GH producing pituitary adenomas in comparison with normal GH cells. Virchows Arch A Pathol Anat Histopathol 411:467–472
35. Navas P, Nowack DD, Morré DJ (1989) Isolation of purified plasma membranes from cultured cells and hepatomas by two-phase partition and preparative free-flow electrophoresis. Cancer Res 49:2147–2156
36. Moran O (2014) On the structural organization of the intracellular domains of CFTR. Int J Biochem Cell Biol 52C:7–14
37. Wang X, Venable J, LaPointe P, Hutt DM, Koulov AV, Coppinger J, Gurkan C, Kellner W, Matteson J, Plutner H, Riordan JR, Kelly JW, Yates JR, Balch WE (2006) Hsp90 cochaperone Aha1 downregulation rescues misfolding of CFTR in cystic fibrosis. Cell 127:803–815
38. Ahner A, Gong X, Frizzell RA (2013) Cystic fibrosis transmembrane conductance regulator degradation: cross-talk between the ubiquitylation and SUMOylation pathways. FEBS J 280:4430–4438
39. Edelman A (2014) Cytoskeleton and CFTR. Int J Biochem Cell Biol 52C:68–72
40. Pranke IM, Sermet-Gaudelus I (2014) Biosynthesis of cystic fibrosis transmembrane conductance regulator. Int J Biochem Cell Biol 52C:26–38
41. Zhang F, Kartner N, Lukacs GL (1998) Limited proteolysis as a probe for arrested conformational maturation of delta F508 CFTR. Nat Struct Biol 5:180–183
42. Bouwstra JA, Gooris GS, Bras W, Talsma H (1993) Small angle X-ray scattering: possibilities and limitations in characterization of vesicles. Chem Phys Lipids 64:83–98
43. Hirai M, Iwase H, Hayakawa T, Koizumi M, Takahashi H (2003) Determination of asymmetric structure of ganglioside-DPPC mixed vesicle using SANS, SAXS, and DLS. Biophys J 85:1600–1610
44. Herbette L, Scarpa A, Blasie JK, Wang CT, Saito A, Fleischer S (1981) Comparison of the profile structures of isolated and reconstituted sarcoplasmic reticulum membranes. Biophys J 36:47–72
45. Chang XB, Hou YX, Riordan JR (1997) ATPase activity of purified multidrug resistance-associated protein. J Biol Chem 272:30962–30968
46. Rich DP, Berger HA, Cheng SH, Travis SM, Saxena M, Smith AE, Welsh MJ (1993) Regulation of the cystic fibrosis transmembrane conductance regulator Cl- channel by negative charge in the R domain. J Biol Chem 268:20259–20267
47. Rich DP, Gregory RJ, Anderson MP, Manavalan P, Smith AE, Welsh MJ (1991) Effect of deleting the R domain on CFTR-generated chloride channels. Science 253:205–207
48. Dulhanty AMRJ (1994) Phosphorylation by cAMP-dependent protein kinase causes a conformational change in the R domain of the cystic fibrosis transmembrane conductance regulator. Biochemistry 33:4072–4079
49. Kanelis V, Hudson RP, Thibodeau PH, Thomas PJ, Forman-Kay JD (2010) NMR evidence for differential phosphorylation-dependent interactions in WT and DeltaF508 CFTR. EMBO J 29:263–277
50. Marasini C, Galeno L, Moran O (2012) Thermodynamic study of the native and phosphorylated regulatory domain of the CFTR. Biochem Biophys Res Commun 423:549–552
51. Baker JMR, Hudson RP, Kanelis V, Choy W, Thibodeau PH, Thomas PJ, Forman-Kay JD (2007) CFTR regulatory region interacts with NBD1 predominantly via multiple transient helices. Nat Struct Mol Biol 14:738–745
52. Lukacs GL, Chang XB, Bear C, Kartner N, Mohamed A, Riordan JR, Grinstein S (1993) The delta F508 mutation decreases the stability of cystic fibrosis transmembrane conductance regulator in the plasma membrane. Determination of functional half-lives on transfected cells. J Biol Chem 268:21592–21598
53. Sharma M, Benharouga M, Hu W, Lukacs GL (2001) Conformational and temperature-sensitive stability defects of the delta F508 cystic fibrosis transmembrane conductance regulator in post-endoplasmic reticulum compartments. J Biol Chem 276:8942–8950
54. Thibodeau PH, Richardson JM, Wang W, Millen L, Watson J, Mendoza JL, Du K, Fischman S, Senderowitz H, Lukacs GL, Kirk K, Thomas PJ (2010) The cystic fibrosis-causing mutation deltaF508 affects multiple steps in cystic fibrosis transmembrane conductance regulator biogenesis. J Biol Chem 285:35825–35835
55. Du K, Sharma M, Lukacs GL (2005) The DeltaF508 cystic fibrosis mutation impairs domain-domain interactions and arrests post-translational folding of CFTR. Nat Struct Mol Biol 12:17–25
56. Pedemonte N, Lukacs GL, Du K, Caci E, Zegarra-Moran O, Galietta LJ, Verkman AS (2005) Small-molecule correctors of defective DeltaF508-CFTR cellular processing identified by high-throughput screening. J Clin Invest. 115:2564–2571 Epub 2005 Aug 25
57. Jurkuvenaite A, Chen L, Bartoszewski R, Goldstein R, Bebok Z, Matalon S, Collawn JF (2010) Functional stability of rescued delta F508 cystic fibrosis transmembrane conductance regulator in airway epithelial cells. Am J Respir Cell Mol Biol 42:363–372
58. Rowe SM, Pyle LC, Jurkevante A, Varga K, Collawn J, Sloane PA, Woodworth B, Mazur M, Fulton J, Fan L, Li Y, Fortenberry J, Sorscher EJ, Clancy JP (2010) DeltaF508 CFTR processing correction and activity in polarized airway and non-airway cell monolayers. Pulm Pharmacol Ther 23:268–278
59. Dalemans W, Barbry P, Champigny G, Jallat S, Dott K, Dreyer D, Crystal RG, Pavirani A, Lecocq JP, Lazdunski M (1991) Altered chloride ion channel kinetics associated with the delta F508 cystic fibrosis mutation. Nature 354:526–528
60. Haws CM, Nepomuceno IB, Krouse ME, Wakelee H, Law T, Xia Y, Nguyen H, Wine JJ (1996) Delta F508-CFTR channels: kinetics, activation by forskolin, and potentiation by xanthines. Am J Physiol 270:C1544–C1555
61. Jih K, Li M, Hwang T, Bompadre SG (2011) The most common cystic fibrosis-associated mutation destabilizes the dimeric state of the nucleotide-binding domains of CFTR. J Physiol 589:2719–2731